2

Conf-941141--3
SAND-94-0761C

THERMOMECHANICAL ANALYSIS OF FAST-BURST REACTORS

Joel D. Miller
Sandia National Laboratories
Department 6514, Mail Stop 1145
Albuquerque, New Mexico 87185-1145
(505) 845-3032

ABSTRACT

Fast-burst reactors are designed to provide intense, short-duration pulses of neutrons. The fission reaction also produces extreme time-dependent heating of the nuclear fuel. An existing transient-dynamic finite element code was modified specifically to compute the time-dependent stresses and displacements due to thermal shock loads of reactors. Thermomechanical analysis was then applied to determine structural feasibility of various concepts for an EDNA-type reactor and to optimize the mechanical design of the new SPR III-M reactor.

I. INTRODUCTION

An important aspect of the design of a pulsed neutron fission reactor is ensuring that its mechanical integrity is maintained during operation. Ideally, all of the stressed components (i.e., the fuel and structural supports) should remain within the elastic material property range for each reactor shot. Unfortunately, the need for high magnitude, short duration pulses conflicts with the mechanical ideal. The role of thermomechanical analysis, therefore, is to optimize the physical design to accommodate high magnitude shots while remaining within safe and repeatable operating limits for the reactor.

Pulse mode operation causes severe thermal transients to arise in the fuel of a fast-burst reactor. A pulse may have a time width at half-maximum power (FWHM) of less than a hundred microseconds, and a maximum fuel-temperature rise of several hundred degrees Celsius within a few hundred microseconds. Large spatial temperature gradients will be produced. The fission heating of the fuel will occur faster than thermal strains can be relieved by material deformation. This thermal shock will produce vibrations leading to high stress in the fuel and supporting structure. For both operational and structural reasons, however, the fuel must be designed to remain in the elastic or near-elastic stress range during a pulse.

In order to predict the mechanical effects due to high-level pulses, an existing finite element method analysis code, PRONTO 3D,[1,2] was modified to calculate thermal shock loadings of fast-burst reactors during pulse mode operation.[3] The modifications consisted of the addition of a thermoelastic material constitutive model and a thermal loading algorithm. Because thermal loads on the typically cylindrical fuel elements are essentially axisymmetric, the load algorithm was formulated to compute temperature distributions within the fuel based on input of normalized radial and axial fission distributions. Although not completely general, this formulation allows virtually any fast-burst type reactor geometry to be analyzed, even with nonsymmetric geometric details.

Two example calculations were used to verify and benchmark the modified code.[3] The first example considered the effects of a reactor pulse on a fuel ring of the proposed but never-built Sandia Pulse Reactor IV (SPR IV). PRONTO 3D results were compared against SPR IV design calculations that were made with the finite difference code STEALTH.[4,5] The second example considered a fissionable solid, slender rod instrumented to measure its temperature and deflection history while subjected to an actual pulse in SPR II.[6] The empirical data from this experiment provided a benchmark for comparison with the PRONTO 3D results.

Thermomechanical studies using PRONTO 3D were done for several reactor designs. Scoping calculations for various configurations of the EDNA (Externally Driven Nuclear Assembly) reactor provided fuel-segmentation and sizing constraint data for conceptual design studies. The finite element based analysis methodology was also used extensively during the design of the new SPR III-M reactor, which is in the final stages of construction.

II. PRONTO 3D CODE MODIFICATIONS

PRONTO 3D is a finite element, three-dimensional Lagrangian transient solid dynamics code developed to

DISCLAIMER

calculate the general displacement behavior of nonlinear or linear materials subjected to high strain rate loading. It uses an explicit time integration method to solve the equations of motion. A thermoelastic constitutive model and spatially variant thermal history load algorithm were added to PRONTO 3D for application to reactor-induced thermal shock problems. The thermoelastic material model was developed to account for temperature dependence of the material properties, including Young's modulus and the coefficient of thermal expansion. The reactor fuel is assumed to behave as an isotropic, homogenous material. The yield stress, if the fuel is a metal such as uranium alloyed with molybdenum, or tensile strength, if it is a ceramic such as uranium carbide or uranium dioxide, also varies with temperature and is accounted for but not used directly in the model. The yield strength is not used to compute plastic deformation, but is tracked as a measure of potential damage to the fuel. A normalized yield/tensile-failure criterion is computed at each time step based on the ratio of the effective stress to the yield or tensile-failure stress.

To be consistent with the preexisting PRONTO 3D formulation, the thermoelastic material model is written in terms of the unrotated Cauchy stress, σ, and the total strain in the unrotated configuration, $\varepsilon = \int \mathbf{d}\,dt$, where $\mathbf{d}$ is the unrotated deformation rate tensor. Stresses are obtained directly from the total unrotated strain, ε:

$$\sigma = \lambda\,(\mathrm{tr}(\varepsilon))\,\delta + 2\mu\varepsilon - (3\lambda + 2\mu)\,\alpha\,(\Delta\Theta)\,\delta \quad (1)$$

where λ and 2μ are the Lamé constants, α is the coefficient of thermal expansion, $\Delta\Theta$ is the temperature rise, and δ is the identity tensor. The Lamé constants are obtained from the more commonly known Young's modulus, E, and Poisson's ratio, υ, as functions of temperature:

$$\lambda(\Theta) = \frac{E(\Theta)\upsilon}{1 - \upsilon - 2\upsilon^2} \quad (2)$$

$$\mu(\Theta) = \frac{E(\Theta)}{2\,(1 + \upsilon)} \quad (3)$$

The driving force is the thermal loading of the fuel due to fissile energy deposition. Energy deposition occurs nonuniformly, creating a time-dependent spatial temperature distribution in the fuel. The temperature history is calculated by Equation (4), which is the integral of a theoretically symmetric function for the power pulse,[7] adjusted for spatial variation based on normalized, independently-computed radial and axial fission distribution functions:

$$\Theta(t) = \frac{E_o \Gamma_r \Gamma_a}{2\,C_p\,V}\left(1 + \tanh\left[\omega\left(\frac{t - \phi\Pi}{2\Pi}\right)\right]\right) + \Theta_o \quad (4)$$

where

- Θ = fuel temperature, in degrees Celsius
- E_o = maximum pulse yield = $(\Theta_{max} - \Theta_o)C_pV$
- Θ_{max} = maximum fuel temperature
- Θ_o = reactor start-up temperature, 25°C in all cases
- C_p = heat capacity of fuel
- V = fuel (individual finite element) volume
- ω = pulse rise-time constant, assumed to be 3.524 radians for SPR III-M
- t = time, in seconds
- ϕ = phase adjustment, assumed to be 2.0 for both EDNA and SPR III-M calculations
- Π = FWHM pulse width, in seconds
- Γ_r = normalized radial fission distribution function
- Γ_a = normalized axial fission distribution function.

The resulting temperature distribution in the fuel is therefore simplified as axisymmetric, with decoupled radial and axial distributions. The magnitude of the thermal load function follows a hyperbolic tangent curve, which can be adjusted for a specific reactor design by specification of four parameters: the maximum temperature rise, the FWHM pulse width, the phase-adjustment constant, and the reactor-dependent rise-time constant.

III. EDNA SCOPING CALCULATIONS

The EDNA concept involves a wide range of reactor sizes and configurations. The feasibility of the EDNA concept was explored with several different fuel materials and for overall reactor dimensions ranging from about 20 cm to several meters. The most basic concept included a large hollow cylinder of fissionable material. Thermomechanical analysis with PRONTO 3D was used to determine the degree of circumferential segmentation necessary for the fuel, since the limiting factor in a cylinder or ring is the hoop stress. Because of the preliminary stage of the investigation, many physical details, such as bearing, friction, or both, between expanding fuel segments, mechanical preloading of the segmented fuel assembly, and interaction with a support structure, which would affect the actual thermomechanical behavior of the fuel elements, were neglected. What was left to analyze were individual, unconstrained pieces of fuel. This had the advantage of allowing many relatively fast calculations to be made with small and simple models.

For example, the finite element mesh for an unsupported (*i.e.*, all boundaries free except for a plane of symmetry) 4-cm by 4-cm by 30° cylindrical fuel segment is shown in Figure 1. In this calculation, the fuel was assumed to be UO_2 and the segment would be located at the axial midplane of the reactor, where fission density is greatest so that both axial and radial temperature gradients aren't significant. Assuming further that the reactor can produce a FWHM pulse of about 81 μs in duration with a maximum temperature rise of about 900°C results in the stress ratio contour plot of Figure 2. The stress contours show a normalized measure of stress, SR, at 200 μs, when the peak tensile stress is reached. SR is the ratio of von Mises (effective) stress to the temperature-dependent tensile strength in each finite element. SR values greater than one mean the tensile strength has been exceeded and that failure is expected (although no cracking behavior occurs in the model). Maximum tensile stresses occur on the outside curvature of the segment. This calculation required less than five minutes of CPU time on a Hewlett-Packard 9000/730-66 workstation.

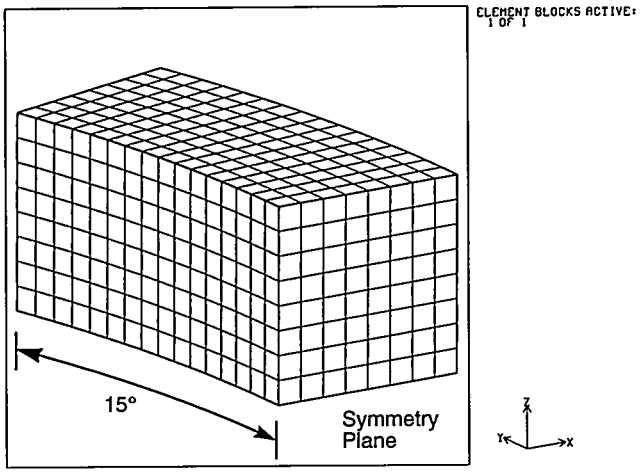

Figure 1. EDNA Fuel Segment Mesh

Parametric studies were conducted in which the segment size, segment shape, pulse width, temperature rise parameters, and material assumptions were varied. For a given set of assumptions regarding the fastest possible pulse for an overall volume of a specific material, the maximum size fuel segment could be determined. For example, the allowable stress curve shown in Figure 3 for the 4-cm by 4-cm UO_2 segment subjected to the pulse discussed above indicates a maximum possible circumferential extent of about 25°.

Because the EDNA reactor concept was at such an early stage of development, a theoretical study of particle

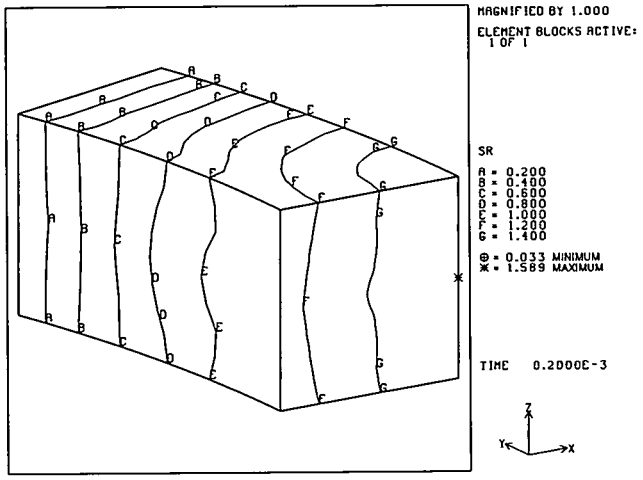

Figure 2. EDNA Fuel Segment Maximum Stress

sizes possible for particular materials over a wide range of pulses was also done. In this set of scoping calculations, particles were assumed to be spherical and uniformly loaded, which kept the number of variables to a minimum. Since a uniformly loaded sphere has no inherently stress-raising geometric feature, an upper bound to particle size, or absolute minimum degree of segmentation could be established.

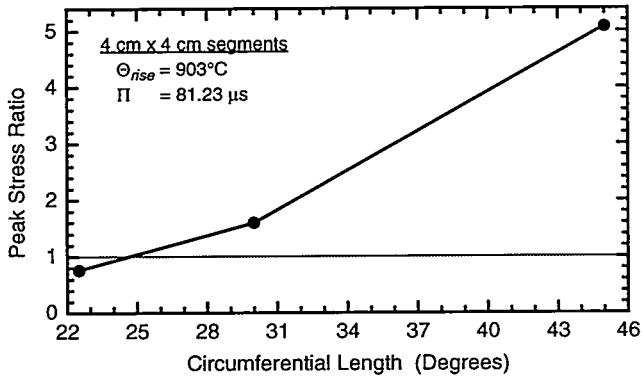

Figure 3. Circumferential Extent vs. Allowable Stress

The results from this study are presented graphically in Figures 4 and 5. These plots show the FWHM pulse width as a function of the largest possible spherical particle for which the peak SR value stays below the failure strength limit of the fuel material, for several levels of temperature rise. The maximum values of temperature rise shown, 900°C for U–10 wt.% Mo and 2100°C for UO_2, correspond to approximately 85% and 75% of the respective melting temperatures of these materials. The ordinate of each plotted point was determined by repeating the PRONTO 3D calculation for the specific pulse

width and temperature rise while changing the dimensions of the sphere until the peak value of SR was computed to be almost exactly one, within a very small tolerance.

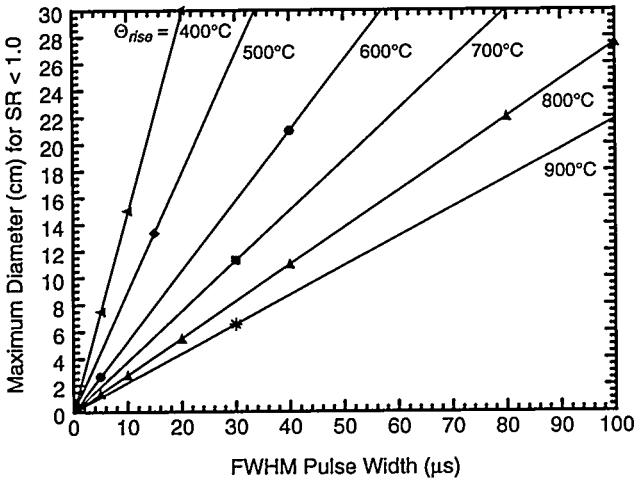

Figure 4. Maximum Size of U–10 wt.% Mo Particles

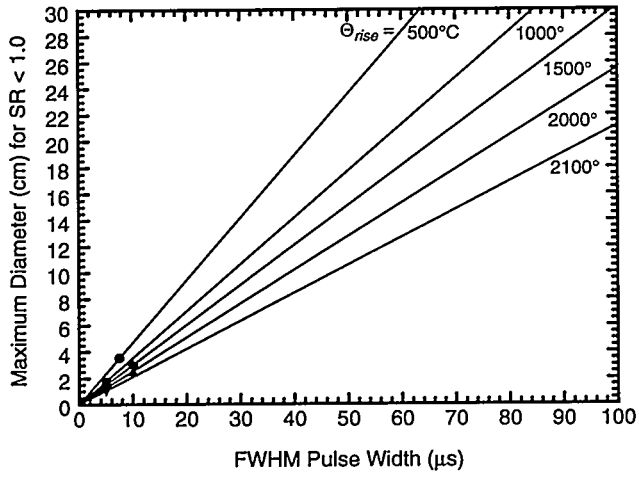

Figure 5. Maximum Size of UO_2 Particles

Although the upper bound particle sizes turned out to be fairly large (*i.e.*, over a centimeter in diameter for pulse widths greater than a few microseconds), in all likelihood an EDNA-type reactor would require a high degree of segmentation. Rectangular cross section segments would have greater stresses than spherical segments of equal volume. Spatial temperature gradients are proportional to flux density and would need to be calculated for a specific configuration. Gradient loading would be more severe than uniform loading. No account was taken of other stress-raising effects such as dynamic contact between fuel pieces or with components of a containing structure if one was necessary. A great deal of uncertainty also exists concerning the material properties at very high temperatures and strain rates. Parametric sensitivity studies would have to be conducted to gauge computational uncertainty, however.

IV. SPR III-M DESIGN CALCULATIONS

The central irradiation cavity of SPR III-M has a diameter of 21 cm and a height of 37 cm. The reactor structure consists of two stacks of fully enriched U–10 wt.% Mo alloy fuel rings held together by stainless steel support rings and bolts. A novel feature of SPR III-M is the incorporation of mechanical springs between the support rings and bolts, the intent of which is to accommodate axial fuel expansion during pulse mode operation without overstressing the support bolts.

Design calculations for SPR III-M were considerably more complicated than the benchmark example problems and EDNA scoping calculations. A stress state will exist in the reactor components prior to any pulse operations as a result of bolt tightening during final assembly. Room-temperature prestress was calculated with the quasi-static finite element code JAC3D[8] and passed to PRONTO 3D as an initial condition using the restart capabilities of the codes. Thermal strains produced by the fuel-temperature rise were calculated with PRONTO 3D for several pulses at the upper limit of the SPR III-M operating range.

The temperature rise caused by fission energy deposition is too rapid for thermal conduction to dissipate the heat energy during the initial vibratory response of the fuel. Therefore, temperature effects in the steel supporting structure of SPR III-M were neglected. Peak stresses from the expansion and contraction phases of the fuel vibrations were determined for both the fuel and supporting structure. By comparing the finite element results from models with successive changes in the fuel rings and steel supporting structure, stresses were reduced to an acceptable level over most of the desired operating regime.

A. SPR III-M Operational Parameters

The relationship between FWHM pulse width and reactor yield, expressed in terms of the peak temperature rise, is plotted in Figure 6. Figure 6 includes the peak temperature rise versus FWHM pulse width relationships for the older, existing SPR III reactor[9] and proposed (but not built) SPR IV reactor.[4] The characteristic curve for SPR III-M was derived by interpolation based on the relative size of each reactor. Because SPR III-M is only slightly larger in cavity diameter than SPR III, the behav-

ior of the newer reactor should be quite similar to the existing one but with slightly longer pulses.

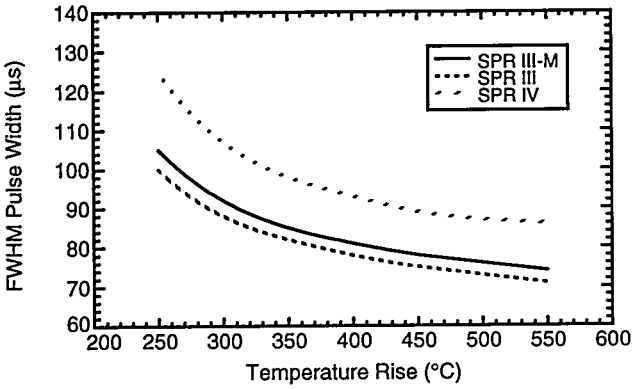

Figure 6. SPR-Type Reactor Pulse Characteristics

SPR III-M fuel temperatures were computed with Equation (4). The spatial distribution of temperature is directly proportional to the fission distribution. Normalized radial and axial fission distribution functions are plotted in Figures 7 and 8. Circumferential variation was neglected. The normalized distribution functions were input to PRONTO 3D as polynomial curve fits, as were the temperature-dependent material properties of the fuel.

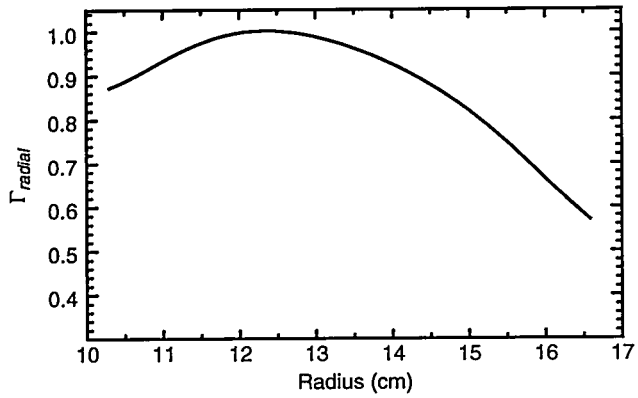

Figure 7. SPR III-M Radial Fission Distribution

B. The Mechanical Design of SPR III-M

The major components at the heart of SPR III-M are the fuel rings, steel support rings, and the large steel bolts that hold the fuel stack assemblies together. There are other components as well, such as gas coolant plenums, neutron reflectors, control rods, and a spider assembly that moves the lower fuel assembly into position to initiate a pulse and then allows it to separate from the upper fuel stack to control neutron multiplication and end the pulse. These other components do not contribute to the structural soundness of the fuel assembly in its capacity to withstand its own pulse loading, however.

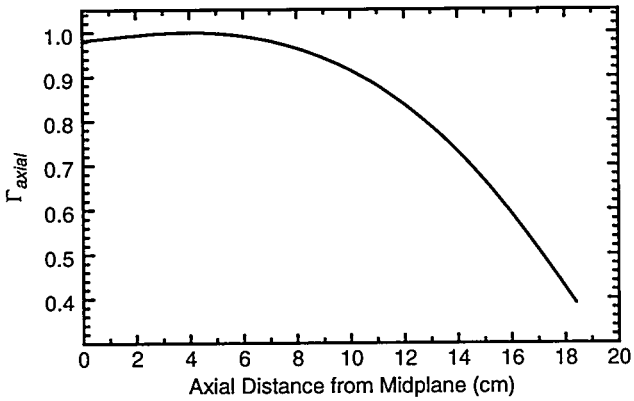

Figure 8. SPR III-M Axial Fission Distribution

The upper and lower fuel assemblies are virtually identical. Each fuel stack (Figure 9) is clamped between two stainless steel support rings by stainless steel bolts situated every 90° around its perimeter. In the original design, the outer support rings incorporated cylindrical pass-through cups holding a stack of Belleville washers on each bolt. The washer stack would be a flexible spring helping the bolt absorb the axial vibration deflections of the fuel assembly. An improved design eliminated the pass-through cups, but not the washer stacks on each bolt.

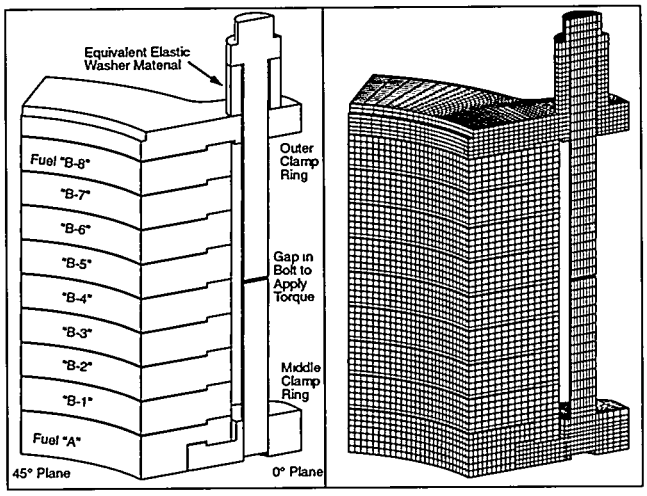

Figure 9. Finite Element Mesh of SPR III-M Final Design

Each cylindrical fuel stack has approximate dimensions of 21 cm across the inner diameter, 33 cm in outer

diameter, and 20 cm in height to the outside of the steel clamp rings. The fuel stacks consist of nine fuel rings plus the upper and lower clamp rings. Eight of the nine fuel rings are identical (shape "B"), while the midplane ring, "A," is shaped differently to allow the midplane steel clamp ring to fit in the stack while also providing a nearly uninterrupted volume of fuel along the inner radius. Small pass-through holes for thermocouples are incorporated in the midplane clamp ring to allow fuel-temperature measurement. The fuel stack assembly incorporates 0.5 mm gaps between each fuel ring, except at the bolt locations every 90° where the rings fit together via lock-tab sections, to allow coolant flow on each ring surface. The designed-in gaps between fuel rings are also intended to reduce axial stress wave propagation.

A total of ten fully coupled static-dynamic numerical simulations of SPR III-M operation were completed, covering four different designs for the reactor. As listed in Table 1, analyses included four yield levels with the initial design, plus simulations comparing the effects of reducing the bolt preload, changing the design to eliminate the Belleville washer stack pass-through cups, and adding more lock-tab features to the outer circumferences of the fuel plates. All together, this resulted in six static JAC3D calculations and ten dynamic PRONTO 3D calculations being made, since identical geometries only required a single bolt preload calculation.

C. SPR III-M Finite Element Models

Virtually identical meshes were used in JAC3D and in PRONTO 3D. Inherent symmetry allowed one-eighth of a fuel assembly (a slice with a 45° circumferential extent) to represent the entire reactor structure. Each numerical model included well over 40,000 nodes and 30,000 eight-node hexagonal elements. The elements were divided among 14 material blocks, including the nine fuel rings, two steel clamp rings, an equivalent-elastic material simulating the Belleville washer stack, and two separate blocks for the single steel bolt. Various contact surfaces either "fixed" components together or allowed intermittent contact between model regions.

Two material blocks were needed to model bolt torquing. An initial dividing gap separating the upper and lower bolt halves equaled the amount of vertical compression specified for the Belleville washers. The quasi-static process of tightening the bolt and compressing the washers proceeded in JAC3D by applying opposite axial displacement functions to each bolt-gap surface boundary. As the two bolt halves were brought into fixed contact, static equilibrium put the bolt in tension and the rest of the model in compression. A restart file was written

Table 1. SPR III-M Operational Case Calculations

Case	Design Model	Reactor Yield (Peak Θ_{rise}) °C	FWHM Pulse Width μs
1	Initial Design	300	92
2		400	81
3		500	76
4		550	74
5	Reduced Preload Reduced spring stiffness (*i.e.*, reduced number of Belleville washers), otherwise same as Case 2.	400	81
6	Alternate Design Bolt preload same as in Case 5, relocated springs to outside of outer, now flat steel clamp ring with longer bolt. Reduced bolt centerline radius about axis of reactor.	400	81
7	Extra Lock Tabs Added locking tabs to fuel at 45° between each bolt, otherwise same as Case 5	400	81
8	Combined Features Similar to Case 6, but added tabs (nonlocking) between bolts every 30° to preserve cooling gaps between stacked fuel plates.	400	81
9	Comb. Features II Same as Case 8, but bolt preload halved.	400	81
10	Comb. Features III Same as Case 8, but without bolt preload.	400	81

and used as input into PRONTO 3D to establish initial stress and displacement conditions. The undeformed mesh for the final design is shown in Figure 9.

The initial reactor design was analyzed over a range of four increasingly severe pulse levels. Subsequent calculations at a constant pulse level of 400°C maximum temperature rise and 81 μs FWHM width investigated de-

sign improvements. Each calculation lasted 650 μs, just long enough to capture a full vibration cycle of the fuel assembly, but short enough to allow neglecting conductive heat transfer from the fuel to the steel components. Only one vibration cycle was examined for two reasons. Because the structural response of succeeding cycles would be dampened by energy-loss mechanisms such as friction and thermal cooling, the highest stresses occur during the first vibration cycle. In addition, each 650 μs PRONTO 3D calculation required about 90 minutes of CPU time on a Cray YMP 8/32 supercomputer.

The first design change (Case 5) reduced the preload on each bolt by decreasing spring stiffness in the stacks of Belleville washers. Changing from sixteen to eight washers per bolt in a reoriented stacking order allowed the same deflection at half the compressive force. The second design change (Case 6) eliminated the cups holding the reduced-height stack of washers by making the outer steel clamping plate entirely flat. This made the outer support rings simpler but had the disadvantage of reducing the axial compactness of the fuel assemblies. The support bolts increased in length although their radial positions decreased relative to the central axis of the reactor. The third change (Case 7) added interlocking tabs to the fuel plates at circumferential intervals halfway between each bolt, which produced more axisymmetric-like radial dynamic deflections. This model was an extension of Case 5 and included the pass-through cups in the outer steel clamping plates. Final geometric changes were incorporated in the models of Cases 8, 9, and 10, which were based on the geometry of Case 6 with the addition of noninterlocking tabs at 30° increments around the outer fuel circumference. Case 9 explored halving the preload of Case 8, while Case 10 dispensed with preload altogether. Case 10 provided an analysis reference point, although a physically unrealistic one since some preload is necessary to keep the bolts from loosening.

D. SPR III-M Finite Element Results

The vibration cycle induced by a reactor pulse consists of three distinct phases. The cycle begins with an initial period of approximately two FWHM pulse widths, in which the fuel starts to expand as the temperature rises halfway to maximum level. Fuel expansion is relatively small, though, as the fuel heats up more rapidly than its inertia allows it to respond. During this time stresses, particularly circumferential stresses, begin to build up. The stresses are initially compressive since the relief provided by expansion lags the rate of heating. By four FWHM pulse widths the temperature rise is complete and the fuel temperature is essentially constant to the end of the calculation. The fuel expands much more, primarily radially, and stresses switch to being tensile and reach their peak shortly after the full temperature rise is completed. Peak stresses occur at the point of maximum deflection, which is the peak radial expansion. The third phase then begins as the fuel rebounds into a radial-compression mode in which the radial deflections reach a minimum point and stresses become compressive. The compressive stress peak occurs at the point of minimum radial deflection. The fuel then continues cycling between tensile and compressive phases, repeating the deflections between maximum and minimum radial expansions. Cyclic axial expansion/contraction phases also occur, although more complex modal behavior is involved because of fuel segmentation along the reactor axis.

The vibratory stress response increases in proportion to the pulse level. Each additional 100°C of temperature rise roughly doubles the mechanical (kinetic) energy level of the vibrations. For the initial design, SR ranges from peak values below 1.0 (all stresses remain elastic) in Case 1 to above 2.0 (widespread yielding) in Case 4. However, some evidence exists that the dynamic (high strain rate) yield strength of U–10 wt.% Mo alloy may be twice the value at quasi-static pull-test rates.[10]

Stress levels were reduced progressively as the design evolved. In all cases, the highest stresses in the fuel occur along the inner radius near the bolts and reactor axial midplane. Figure 10 is a typical plot of stress (SR, Case 9) at the tensile-phase peak. High tensile stress is more likely to cause cracks than compressive stress, thus is of more concern. Maximum significant dynamic stresses and strains from calculations at identical pulse levels are listed in Table 2, which shows the progressive improvement as the design changes were implemented in the models. Stresses are most notably lowered by the Case 7 model due to its more uniform deflections, followed by Case 9, which has similar geometry and further reduced preload (Case 10 is not realistic, since it did not include any bolt preload on the fuel assembly). Cases 7 and 9 also result in the least localized yielding of the steel components. Some yielding is indicated in every design, but far less with the improved designs. At worst, in the later designs, yielding is confined to localized strain hardening of the stainless steel middle support ring, mainly in the thermocouple holes (which would deform by closing less than two percent of their nominal 3-mm diameter in the worst case investigated, Case 4). In no case did the average cross-sectional bolt stresses come close to yielding.

V. CONCLUSION

Thermal shock stress in the fuel and structure of a fast-burst reactor must be determined in order to allow it

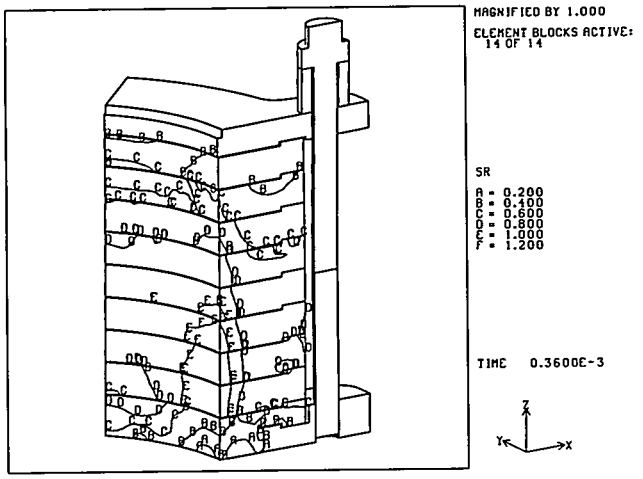

Figure 10. Peak Tensile SR Contours, SPR III-M Case 9

to operate safely and reliably. The deleterious mechanical effects of high magnitude, short duration pulses may be quite severe and must be accounted for in the design process. Analysis methodology based on modifications incorporated into the transient-dyanmic finite element code PRONTO 3D was developed to address reactor-induced thermal shock loading. Thermomechanical analysis with three-dimensional finite element codes is advantageous in that it accounts for all important geometric details in a design. The capability was instrumental in analyzing mechanical behavior and reducing stresses significantly in the nonaxisymmetric design of the new SPR III-M reactor. Thermomechanical analysis also had a major impact in determining the feasibility of various EDNA reactor designs. Although EDNA design work has not progressed beyond the feasibility stage, valuable insight was gained concerning the degree of fuel segmentation that would be necessary to build such a reactor.

Table 2. SPR III-M Stress/Strain Results

Case	Tensile Phase (t = 360 μs)		Compressive Phase (t = 560 μs)	
	Peak SR (Fuel)	Peak ε_p (Steel)	Peak SR (Fuel)	Peak ε_p (Steel)
2	1.330	1.11%	1.397	1.57%
5	1.284	0.92%	1.391	1.34%
6	1.269	0.87%	1.395	1.28%
7	1.051	0.69%	1.250	0.90%
8	1.209	0.68%	1.397	0.88%
9	1.189	0.65%	1.391	0.93%
10	1.146	0.05%	1.342	1.13%

ACKNOWLEDGMENTS

This work was performed for the United States Department of Energy under Contract No. DE-AC04-84AL85000.

REFERENCES

1. L. M. Taylor and D. P. Flanagan, "PRONTO 3D: A Three-Dimensional Transient Solid Dynamics Program," SAND87-1912, Sandia National Laboratories, Albuquerque, New Mexico (1989).

2. S. W. Attaway, "Update of PRONTO 2D and PRONTO 3D Transient Solid Dynamics Program," SAND90-0102, Sandia National Laboratories, Albuquerque, New Mexico (1990).

3. D. S. Oscar, S. W. Attaway, and J. D. Miller, "Modifications of the PRONTO 3D Finite Element Program Tailored to Fast Burst Nuclear Reactor Design," SAND91-0959, Sandia National Laboratories, Albuquerque, New Mexico (1991).

4. J. S. Philbin, J. L. Tills, T. F. Luera, and T. R. Schmidt, "Description and Analysis of Sandia Pulse Reactor-IV (SPR-IV)," SAND82-0445, Sandia National Laboratories, Albuquerque, New Mexico (1982).

5. R. Hofmann, "STEALTH—A Lagrange Explicit Finite Difference Code for Solids, Structural, and Thermohydraulic Analysis," EPRI NP-2080-CCM, Science Applications Incorporated, San Leandro, California (1981).

6. J. A. Reuscher and T. R. Schmidt, "Material Property Determination for Fast Pulsed Reactor Fuels by Rapid Fission Heating," *Nucl. Technol.*, **28**, 57 (1976).

7. J. A. Reuscher, "Analysis of Internal Heating Shock Effects in Reactor Fuel Components," *Nucl. Engineering and Design*, **18**, 213 (1972).

8. J. H. Biffle, "JAC3D—A Three-Dimensional Finite Element Computer Program for the Nonlinear Quasi-Static Response of Solids with the Conjugate Gradient Method," SAND87-1305, Sandia National Laboratories, Albuquerque, New Mexico (1987).

9. L. L. Bonzon, B. F. Estes, J. S. Philbin, and J. A. Reuscher, "Sandia Pulse Reactor-III (SPR-III): Safety Analysis Report," SLA-74-0349, Sandia National Laboratories, Albuquerque, New Mexico (1974).

10. K. G. Hoge, "Some Mechanical Properties of Uranium–10 wt Percent Molybdenum Alloy Under Dynamic Tension Loads," *Proc. ASME Metals Engineering and Production Engineering Conf.*, Berkeley, California, ASME 65-MET-8, (1965).